ACADEMIA ROMÂNĂ
Revue Roumaine de Chimie
https://www.icf.ro/rrch/

Rev. Roum. Chim.,
2026, *71*(5–6), 399–411
DOI: 10.33224/rrch.2026.71.5-6.10

COMPUTATIONAL ANALYSIS OF ANTI-HIV-1 DRUG, RILPIVIRINE INTERACTION WITH HUMAN SERUM ALBUMIN

Mohammed Qadir SAEED,[a] Fazal REHMAN,[b] Adyani Azizah Abd. HALIM,[c] Saharuddin B. MOHAMAD,[b] Mujaheed ABUBAKAR,[d] Kushagra KHANNA,[a] Mogana S. RAJAGOPAL[a] and Saad TAYYAB[a*]

[a] Faculty of Pharmaceutical Sciences, UCSI University, Bandar Springhill Campus, 71010 Port Dickson, Negeri Sembilan, Malaysia
[b] Institute of Biological Sciences, Universiti Malaya, 50603 Kuala Lumpur, Malaysia
[c] Department of Oral and Craniofacial Sciences, Faculty of Dentistry, Universiti Malaya,50603 Kuala Lumpur, Malaysia
[d] Department of Biological Sciences, Faculty of Natural and Applied Sciences, Sule Lamido University, Kafin Hausa, Nigeria

Received February 8, 2026

Rilpivirine (RPV), an anti-HIV-1 drug, is a non-nucleoside reverse transcriptase inhibitor and exhibits extensive plasma albumin association; however, the structural basis of this interaction remains unclear. Here, molecular docking and molecular dynamics (MD) simulations were used to examine how binding-site context and ligand occupancy influence plausible RPV binding modes on human serum albumin (HSA). Docking was performed across the three principal albumin binding regions using ligand-free HSA structure (PDB ID: 1BM0) and ligand-occupied HSA structures containing warfarin (PDB ID: 2BXD), diazepam (PDB ID: 2BXF), or bilirubin (PDB ID: 2VUE). In ligand-free HSA, RPV showed a consistent energetic preference for subdomain IB (Site III), and this preference was largely retained in the warfarin- and diazepam-bound structures. In contrast, bilirubin occupancy altered the accessible binding landscape and redirected binding toward alternative regions. A 100 ns MD simulation of the Site III complex supported overall structural stability and persistent ligand confinement. These findings provide a conservative, structure-informed framework for interpreting RPV–HSA interactions and motivate targeted experimental validation.

INTRODUCTION

Despite major therapeutic advances, human immunodeficiency virus (HIV) infection remains a significant global health challenge. At the end of 2024, an estimated 40.8 million people worldwide were living with HIV, a disease that was once considered uniformly fatal prior to the introduction of antiretroviral therapy (ART) in the late 1980s and, especially, effective combination therapy in the mid-1990s.[1,2] Among currently available ART agents, rilpivirine (RPV) is a second-generation non-nucleoside reverse transcriptase inhibitor (NNRTI) belonging to the diarylpyrimidine chemical class (Fig. 1). RPV inhibits viral replication by binding to an allosteric site on HIV-1 reverse transcriptase, thereby preventing viral DNA polymerization.[3] Approved by the U.S. Food and Drug Administration (FDA) in 2011, RPV is administered as part of combination regimens in

* Corresponding author: Saad.Tayyab@ucsiuniversity.edu.my

once-daily oral formulations or as long-acting injectable combinations given monthly or bimonthly, enabling simplified dosing strategies and improved treatment adherence.[4,5]

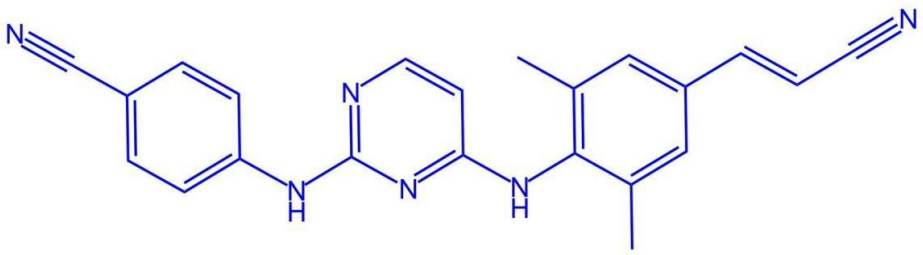

Fig. 1 – Chemical structure of rilpivirine (RPV).

Following administration, RPV reaches peak plasma concentration approximately four to five hours post-dose and exhibits an elimination half-life of about 45 h.[6] In plasma, RPV is extensively protein-bound (~99.7%), predominantly to human serum albumin (HSA), with a minor contribution from α_1-acid glycoprotein.[4,7] Such extensive plasma protein binding is a key determinant of drug distribution, apparent clearance, and systemic exposure, and may influence pharmacokinetic variability and drug-drug interaction potential.[8]

Human serum albumin, the most abundant plasma protein in circulation (35–50 g L^{-1}), serves as a principal transport protein for endogenous ligands and numerous exogenous compounds, including drugs.[9] Structurally, HSA is composed of three homologous domains (I–III), each subdivided into A and B subdomains, forming a globular tertiary structure that enables versatile ligand accommodation.[10] Three major ligand-binding regions have been characterized: Sudlow's Site I in subdomain IIA, Sudlow's Site II in subdomain IIIA, and an additional prominent binding region, Site III in subdomain IB, which serves as the primary site for bilirubin and hemin.[11–14] These sites differ in shape, polarity, ligand preference, and ligand occupancy – particularly by high-affinity endogenous compounds such as bilirubin, which can modulate the accessibility and binding behavior of neighboring regions due to the dynamic and allosterically coupled nature of the protein.[12,14] Although the extent of RPV plasma protein binding has been quantified using equilibrium dialysis across clinically relevant concentration ranges, the molecular basis of its interaction with HSA – including binding-site context and residue-level interactions – has not been structurally characterized.[15] Elucidating these features is relevant for understanding potential competitive interactions in polypharmacy settings and for anticipating pharmacokinetic variability under altered physiological conditions.[16]

Computational approaches such as molecular docking provide a practical framework for probing drug-protein interactions by predicting ligand orientations and interaction patterns within defined binding cavities[17] and have been widely applied to albumin-drug systems.[18] In the present study, molecular docking was employed to investigate the binding behavior of RPV across the three principal HSA binding regions using ligand-free HSA (PDB ID: 1BM0) together with ligand-occupied structures containing warfarin (PDB ID: 2BXD), diazepam (PDB ID: 2BXF), or bilirubin (PDB ID: 2VUE). This approach enabled comparison of site preference and interaction patterns under distinct occupancy states. To complement the static nature of docking calculations and to assess the dynamic stability of the selected binding mode, molecular dynamics simulations were subsequently performed on the RPV-HSA complex, providing time-resolved insight into conformational stability and protein-ligand interactions.

EXPERIMENTAL

Protein Selection and Preparation

Four X-ray crystal structures of human serum albumin (HSA) were retrieved from the Protein Data Bank (PDB);[19] 1BM0 (ligand-free),[20] 2BXD (warfarin-bound),[14] 2BXF (diazepam-bound),[14] and 2VUE (bilirubin-bound).[21] Only chain A was used for all docking calculations. Protein preparation was carried out using AutoDock 4.2.6 and AutoDock Tools (ADT) version 1.5.7.[22] All crystallographic water molecules were removed, polar hydrogens were added, Kollman charges were assigned, and non-polar hydrogens were merged. The prepared receptor structures were saved in PDBQT format for subsequent docking simulations.

Ligand Preparation

The three-dimensional structure of RPV was generated and subsequently geometry-optimized using Avogadro (version 1.2.0) with the MMFF94 force field under default convergence criteria.[23] The optimized structure was saved in PDB format and imported into ADT 1.5.7, where Gasteiger charges were assigned, ligand flexibility was defined (five active torsional bonds), and the final ligand structure was exported in PDBQT format.

Docking Protocol, Analysis, and Visualization

Molecular docking simulations were performed using AutoDock 4.2.6 with ADT for grid and parameter setup. Docking was carried out for Sudlow's Sites I and II as well as Site III (subdomain IB) regions in all four protein structures (1BM0, 2BXD, 2BXF, 2VUE). For each predefined binding site, a grid box of 70×70×70 points with a spacing of 0.375 Å was employed to ensure complete coverage of the binding pocket. Grid centers were defined based on key residues reported to interact with site-specific marker ligands: Trp214 and Tyr150 for Sudlow's Site I (warfarin-binding),[14] Arg410 and Tyr411 for Sudlow's Site II (diazepam-binding),[14] and Tyr138, Tyr161, and Lys190 for Site III (bilirubin-binding).[21] Grid placement was manually inspected to avoid overlap with adjacent binding regions.

Docking calculations were conducted using the Lamarckian Genetic Algorithm (LGA) with 100 independent runs per binding site for each protein structure. Each run was limited to a maximum of 2.5×10^6 energy evaluations, with a population size of 150 individuals, a maximum of 27,000 generations, a mutation rate of 0.02, and a crossover rate of 0.8 (default AutoDock parameters). Docking results were saved in DLG format for analysis, and representative docked poses were exported in PDB format.

Docking outputs were clustered using the default AutoDock RMSD tolerance of 2.0 Å. For each cluster, the lowest and mean binding energies were extracted and compared. Cluster distribution and binding energy plots were generated using OriginPro, version 2025b.[24] Three-dimensional inspection of docked poses was performed using ChimeraX (version 1.10.1)[25] to assess spatial compatibility within the binding pockets, while LigPlot+ [26] was used to generate two-dimensional diagrams of intermolecular interactions.

Molecular Dynamics Simulations

Molecular dynamics (MD) simulations were performed to evaluate the time-dependent binding stability and conformational behavior of the docked RPV-HSA complex (Site III pose in 1BM0). Simulations were carried out using GROMACS 2023.3[27] with the CHARMM36 (July 2022) force field.[28] The complex was placed in a periodic simulation box (approximately 11.40 × 11.40 × 8.06 nm) and solvated using the TIP3P water model.[29] Ligand topology and parameters were generated using SwissParam[30] and incorporated into the system topology.

Energy minimization was performed prior to equilibration. The system was equilibrated under NVT conditions for 0.2 ns (dt = 1 fs) using the V-rescale thermostat at 300 K,[31] followed by NPT equilibration for 0.5 ns (dt = 2 fs) using the V-rescale thermostat and the Parrinello-Rahman barostat at 1 bar.[32] Production MD was performed for 100 ns using a 2 fs time step, with long-range electrostatics treated using the particle-mesh Ewald method[33] and a Verlet cutoff scheme. Coordinates were saved every 10 ps in compressed trajectory format, yielding 10,001 frames over the 0–100 ns simulation for subsequent analysis. Trajectory analyses (including RMSD, RMSF, radius of gyration, intermolecular hydrogen bonds, and minimum distance metrics) were calculated from the RPV-HSA complex trajectory; with RMSD and RMSF reported for HSA after least-squares fitting to the protein backbone of the starting structure.

RESULTS AND DISCUSSION

Docking of Rilpivirine to Ligand-Free HSA (1BM0)

Docking of rilpivirine (RPV) to ligand-free HSA structure (PDB ID: 1BM0) revealed clear site-dependent differences in binding energetics across the three principal drug-binding regions (Sites I–III). Cluster analysis distinctly identified Site III as the most energetically and structurally consistent binding region for RPV (Fig. 2). The distribution of mean binding energies varied markedly among three sites, with Site III (subdomain IB) exhibiting a pronounced shift toward more favorable (more

negative) energy values compared to Sudlow's Sites I and II. At Site III, the dominant cluster comprised 38 docked poses with a mean binding energy of −41.84 kJ/mol, indicating recurrent sampling of a similar low-energy binding mode. In contrast, docking at Sites I and II resulted in more dispersed clustering patterns (Fig. 2), with fewer poses contributing to any single low-energy cluster and a broader overall energy distribution, consistent with weaker and less well-defined binding preferences. Furthermore, the lowest binding energy observed at Site III was −45.19 kJ/mol, exceeding the most favorable poses identified at Site I (−37.28 kJ/mol) and Site II (−29.04 kJ/mol). Based on these results, conformation with the lowest binding energy at Site III was selected for orientation analysis.

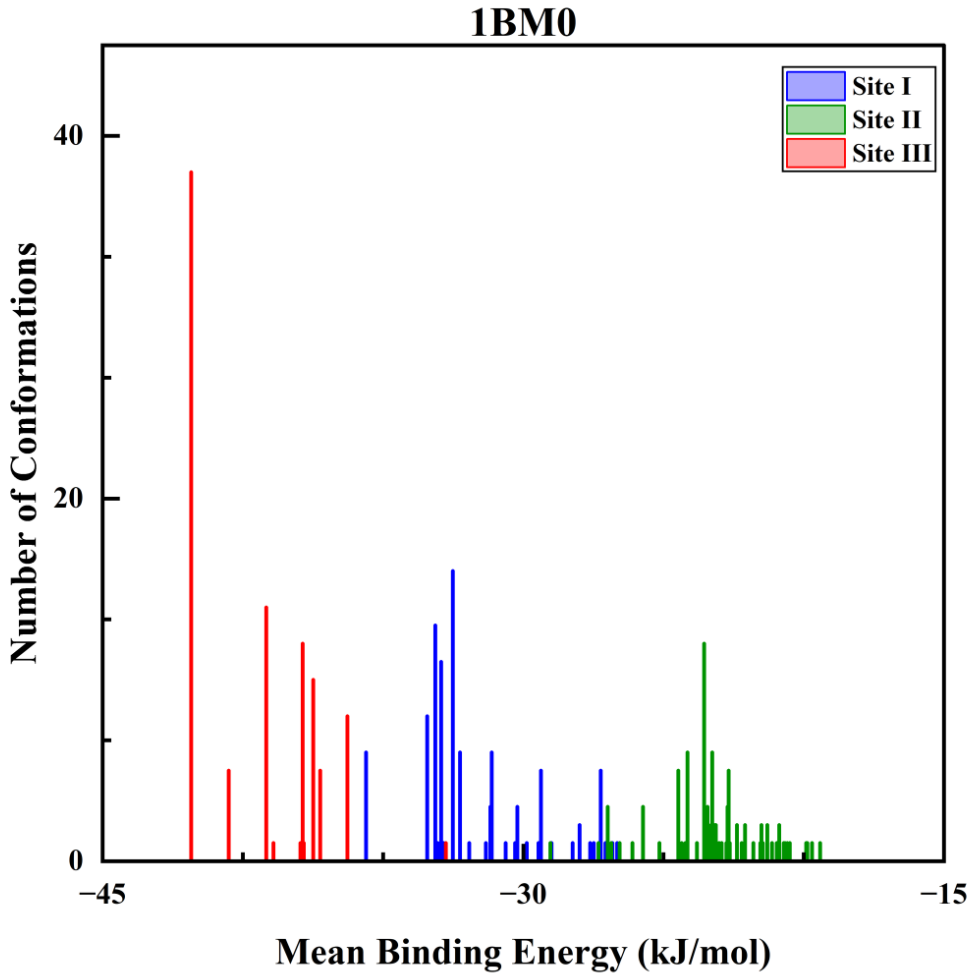

Fig. 2 – Distribution of mean binding energies obtained from docking of RPV to ligand-free HSA (PDB ID: 1BM0) at three principal binding regions. The numbers of docked conformations as a function of mean binding energy are shown for Site I **(**blue), Site II (green), and Site III (red).

Structural inspection of the representative Site III pose (Fig. 3) showed RPV accommodated within a compact pocket in subdomain IB. The ligand was primarily stabilized through hydrophobic contacts (Fig. 3B), complemented with a hydrogen bond involving N5 atom of RPV and phenolic -OH group of Tyr138 of HSA (Figs. 3A and B). LigPlot+ analysis revealed that 16 residues of HSA, *viz.*, Leu115, Arg117, Met123, Phe134, Lys137, Glu141, Ile142, His146, Phe149, Tyr161, Leu182, Leu185, Arg186, Gly189, Lys190 and Ser193 surrounding RPV formed hydrophobic contacts (Fig. 3B). This interaction pattern provides a structural basis for the favorable energetics and high cluster convergence observed at Site III. Taken together, the combined analysis of clustering behavior, energy distributions, and intermolecular interactions indicated that subdomain IB (Site III) represented the most favorable and consistently sampled binding region for RPV in the ligand-free HSA structure.

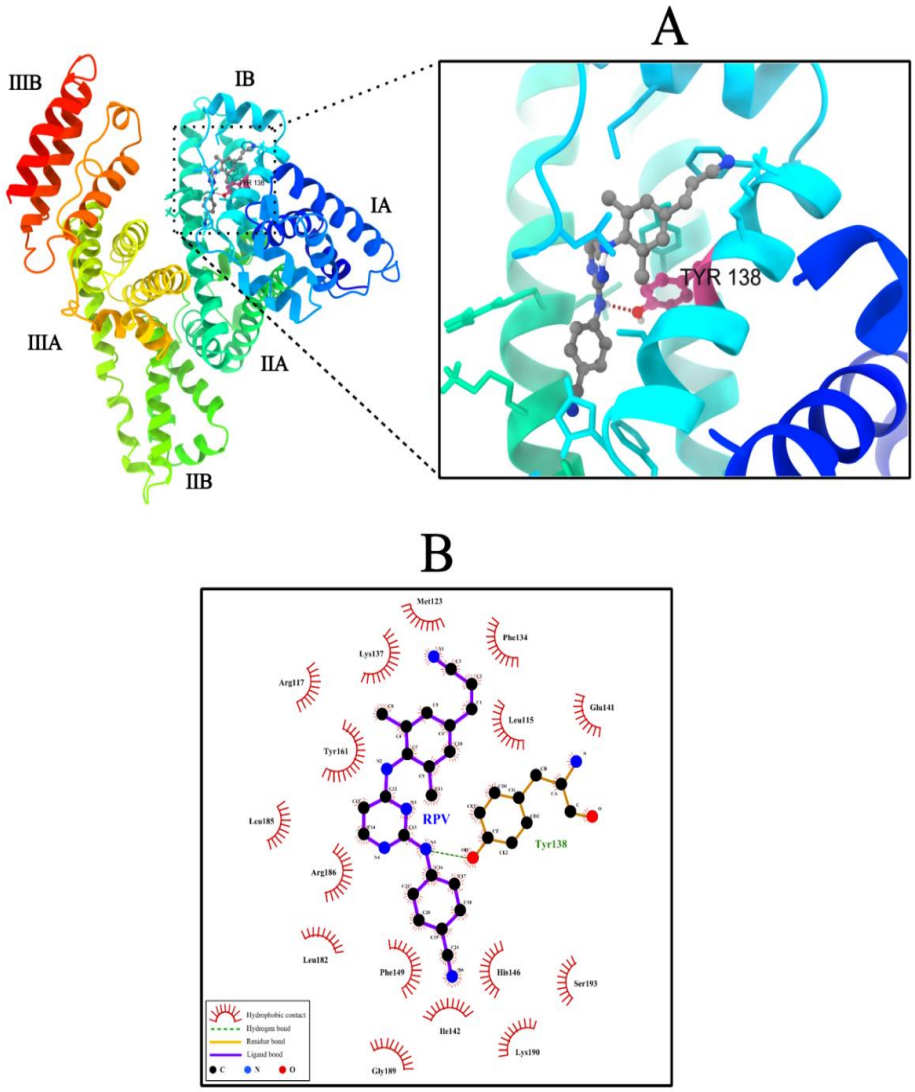

Fig. 3 **–** Representative docked pose of RPV within subdomain IB (Site III) of ligand-free HSA (PDB ID: 1BM0): A**)** Three-dimensional view of the RPV-HSA complex highlighting the location of Site III within HSA domain architecture, and a zoomed view of the binding pocket; B**)** LigPlot+ diagram illustrating key intermolecular contacts between RPV and surrounding residues at Site III.

Docking of Rilpivirine to Warfarin- and Diazepam-Bound HSA Structures

To further examine how occupancy of the canonical Sudlow drug-binding regions influences the accessible binding landscape for rilpivirine (RPV), site-specific docking was additionally performed using warfarin-bound (PDB ID: 2BXD) and diazepam-bound (PDB ID: 2BXF) HSA structures.

In the warfarin-bound HSA structure (2BXD), docking results remained clearly site-dependent (Fig. 4). At Sudlow's Site I (subdomain IIA), the lowest-energy pose reached −33.18 kJ/mol, while the dominant cluster comprised 48 docked conformations with a mean binding energy of −31.67 kJ/mol. Docking at Sudlow's Site II (subdomain IIIA) produced a more dispersed clustering pattern, with the lowest-energy pose reaching −38.49 kJ/mol and the dominant cluster of 27 conformations exhibiting a mean binding energy of −33.76 kJ/mol. By contrast, Site III (subdomain IB) again showed the most favorable and structurally consistent binding profile. The dominant cluster at Site III comprised 28 docked poses with a mean binding energy of −38.91 kJ/mol, while the most favorable pose reached −40.79 kJ/mol. These results indicate that occupancy of Site I by warfarin did not abolish favorable accommodation of RPV elsewhere on protein and that Site III remained the most energetically preferred region under these conditions.

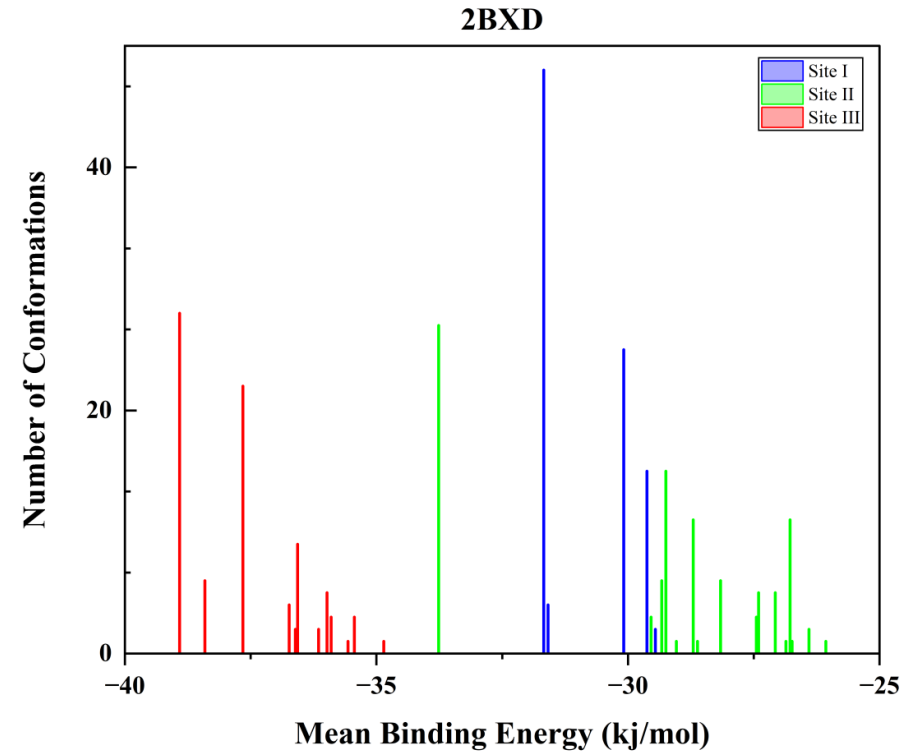

Fig. 4 – Distribution of mean binding energies obtained from docking of RPV to warfarin-bound HSA (PDB ID: 2BXD) at three principal binding regions. The numbers of docked conformations as a function of mean binding energy are shown for Site I (blue), Site II (green), and Site III (red).

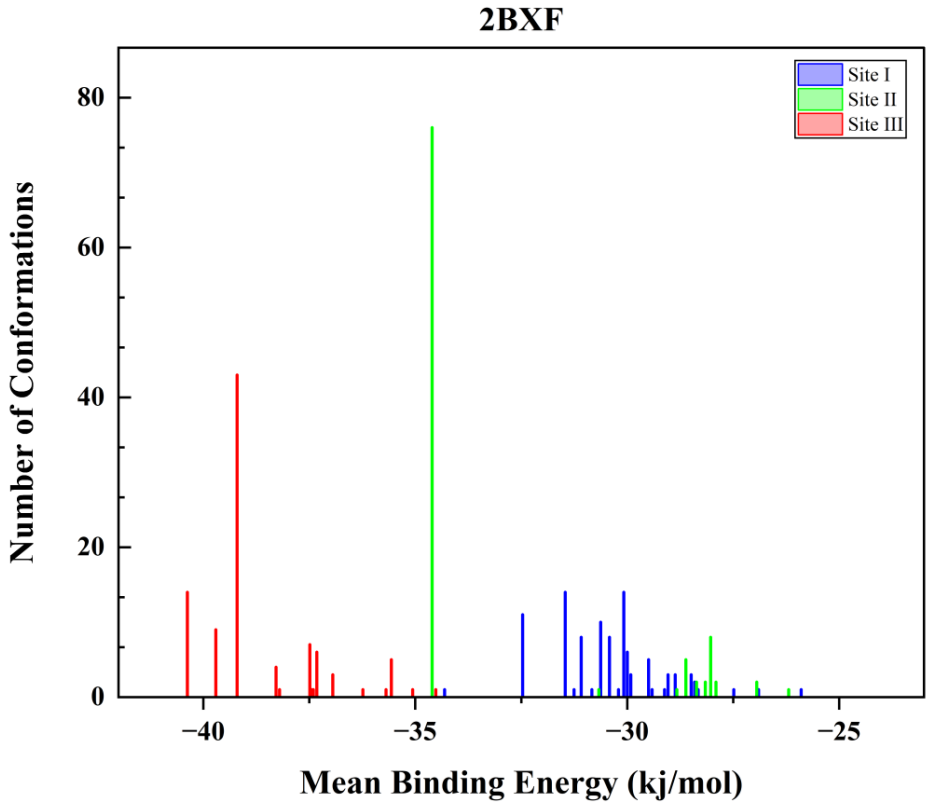

Fig. 5 – Distribution of mean binding energies obtained from docking of RPV to diazepam-bound HSA (PDB ID: 2BXF) at three principal binding regions. The numbers of docked conformations as a function of mean binding energy are shown for Site I (blue), Site II (green), and Site III (red).

A similar trend was observed for the diazepam-bound HSA structure (2BXF) (Fig. 5). At Sudlow's Site I, the lowest-energy pose reached −34.31 kJ/mol, and the dominant cluster of 14 docked conformations showed a mean binding energy of −31.46 kJ/mol. Docking at Sudlow's Site II generated a large dominant cluster comprising 76 poses with a mean binding energy of −34.60 kJ/mol, while the most favorable pose reached −36.78 kJ/mol. Although this substantial cluster size indicates that RPV can be reproducibly accommodated within the Site II search region under diazepam-bound conditions, the corresponding binding energies remained less favorable than those observed for Site III. In subdomain IB, the dominant cluster comprised 43 docked conformations with a mean binding energy of −39.20 kJ/mol, and the lowest-energy pose reached −42.84 kJ/mol, again identifying Site III as the most favorable binding region in this receptor state.

The representative Site III poses obtained from 1BM0, 2BXD, and 2BXF are compared in Fig. 6. Superposition showed that RPV adopted a broadly similar orientation within subdomain IB across the ligand-free, warfarin-bound, and diazepam-bound structures, supporting preservation of a common low-energy binding mode when Site III remained unoccupied. In the diazepam-bound structure, the representative pose was supported by a hydrogen bond with Tyr161 together with hydrophobic contacts involving residues such as Ile142, Phe134, and Lys190, whereas in the warfarin-bound structure the representative pose was likewise stabilized by interactions with residues lining the Site III cavity, including Tyr138, Ile142, and Lys190. Taken together, the results obtained from 2BXD and 2BXF indicate that pre-occupation of Sudlow's Site I or Site II does not eliminate the energetic preference of RPV for subdomain IB. Rather, across both marker-bound structures, Site III remained the most favorable and consistently sampled binding region, whereas docking within Sites I and II was comparatively weaker or more dependent on local structural constraints imposed by the co-crystallized ligand.

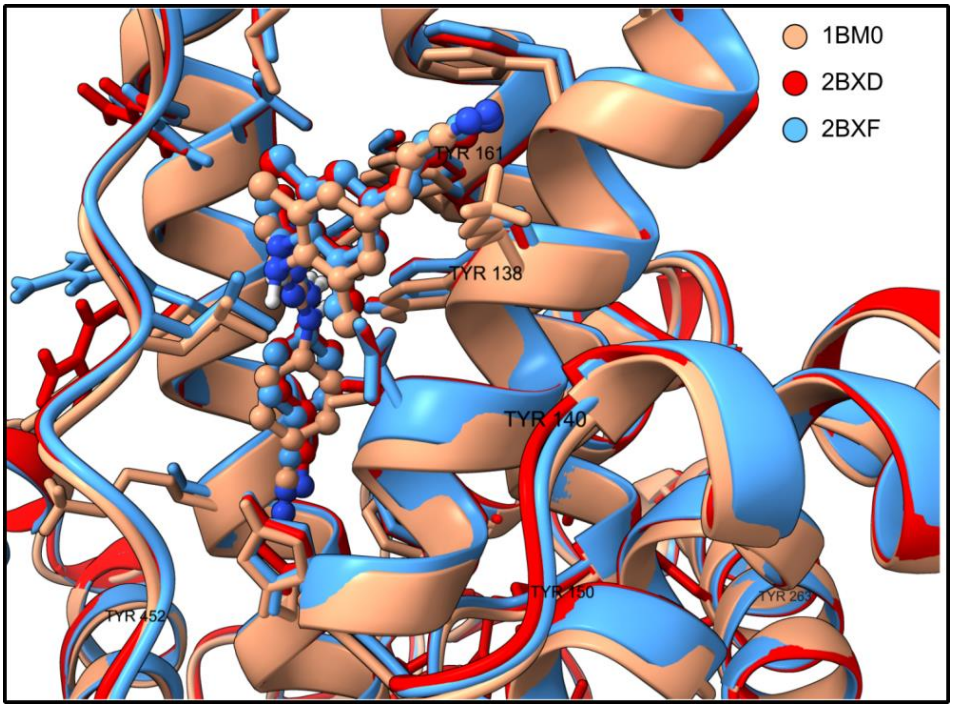

Fig. 6 – Superposition of representative Site III docking poses. The overlay shows the representative Site III poses obtained from ligand-free HSA (1BM0), warfarin-bound HSA (2BXD), and diazepam-bound HSA (2BXF).

Docking of Rilpivirine to Site III-Occupied HSA (2VUE)

Docking of rilpivirine (RPV) to Site III specific ligand, bilirubin-bound HSA structure (PDB ID: 2VUE) revealed a redistribution of favorable binding modes compared to the ligand-free protein, reflecting the altered accessibility of the binding regions upon endogenous ligand occupancy. As illustrated in Fig. 7, site-dependent differences in

the binding energetics and clustering behavior were observed across Sudlow's Sites I and II and the Site III (subdomain IB)-adjacent region.

At Sudlow's Site I (subdomain IIA), docking resulted in a broad distribution of clusters with modest energetic preference. The lowest-energy pose exhibited a predicted binding energy of −36.6 kJ/mol, while the dominant cluster (16 poses) displayed a mean binding energy of −32.1 kJ/mol (Fig. 7). The fragmented clustering pattern and relatively shallow energy distribution suggested that Site I did not constitute a strongly preferred binding region for RPV in the bilirubin-bound HSA. In contrast, docking at Sudlow's Site II (subdomain IIIA) yielded more convergent results. The most favorable pose reached −35.6 kJ/mol, and the dominant cluster comprised 33 docked conformations with a mean binding energy of −34.3 kJ/mol (Fig. 7). Structural inspection of the representative pose (Figs. 8A; 8B) showed RPV partially buried within the Site II cavity and stabilized by a combination of hydrophobic contacts and polar interactions (Fig. 9A). The pronounced cluster convergence and depth of ligand accommodation supported Site II as a favorable binding region for RPV in the presence of bilirubin.

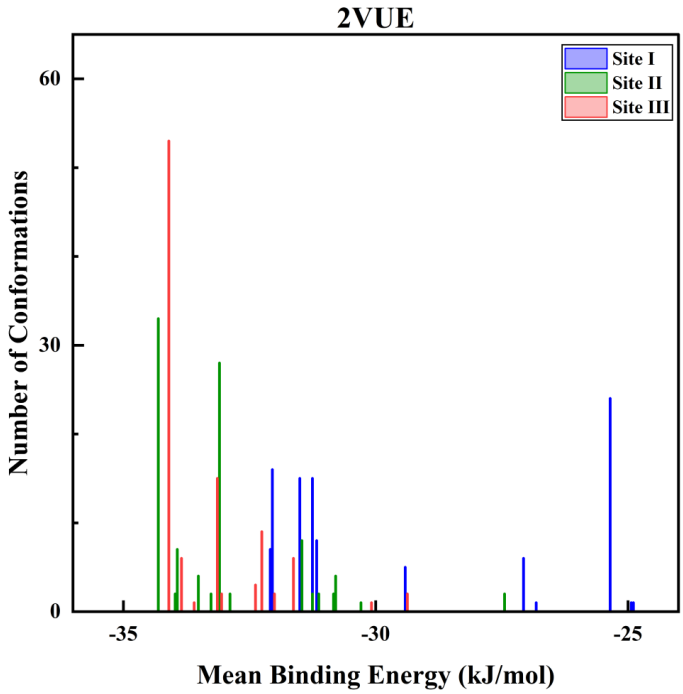

Fig. 7 – Cluster distribution of docking conformations for RPV at three principal drug-binding sites of bilirubin-bound HSA (PDB ID: 2VUE). Sudlow's Site I (subdomain IIA), Sudlow's Site II (subdomain IIIA), and Site III (subdomain IB; bilirubin/hemin-binding site) are shown in blue, green and pink colors, respectively.

Docking runs initiated toward Site III (subdomain IB), which is occupied by bilirubin in the 2VUE structure, identified an alternative binding mode localized to a peripheral region spanning the IA/IB interface. Although the lowest-energy pose in this region reached −36.2 kJ/mol, the dominant cluster (53 poses) exhibited a mean binding energy of −34.1 kJ/mol (Fig. 7). The representative pose (Figs. 8C; 8D) adopted a shallow orientation at the domain interface, stabilized by a hydrogen bond with Glu17 and surrounding hydrophobic residues, as further detailed in the corresponding interaction map (Fig. 9B). This binding mode likely reflects accommodation at an adjacent surface-accessible region rather than occupation of the canonical bilirubin-binding pocket itself. Taken together, these results indicated that bilirubin occupancy reshaped the binding landscape available to RPV, disfavoring canonical Site III (subdomain IB) binding while permitting energetically comparable interactions at alternative regions. Among the sampled sites, Sudlow's Site II emerged as the most structurally and energetically consistent binding region for RPV in the bilirubin-bound HSA structure, whereas interactions at the IA/IB interface appear more surface-associated and potentially less constrained.

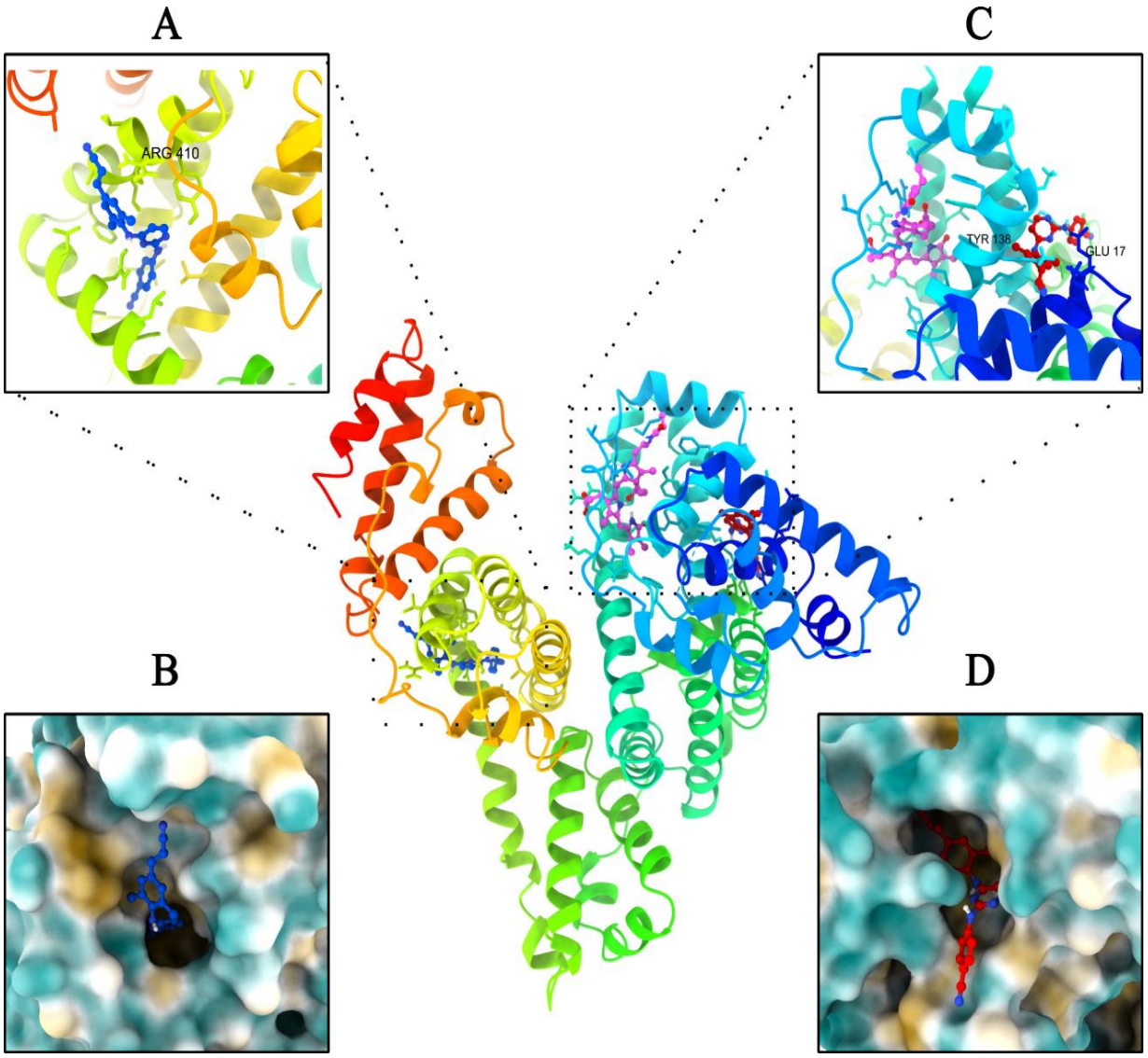

Fig. 8 – Docking-derived binding poses of RPV on bilirubin-bound HSA (PDB ID: 2VUE). The central panel shows the overall HSA structure in ribbon representation, with the location of the docked RPV poses indicated: A) Close-up view of a representative docked pose of RPV at Sudlow's Site II (subdomain IIIA), with nearby residue labeled; B) Surface representation of Sudlow's Site II showing the position of the docked RPV pose within the binding cavity: C) Close-up view of an alternative docked pose located near the IA/IB interface adjacent to the bilirubin-binding region (Site III), with selected residues labeled; D) Corresponding surface representation of the IA/IB interface showing the spatial location of the docked RPV pose. All poses correspond to representative docking conformations obtained from site-specific docking calculations.

From a pharmacokinetic perspective, the repeatedly favorable accommodation of RPV within subdomain IB (Site III) in ligand-free, warfarin-bound, and diazepam-bound HSA suggests that this region may represent a relevant albumin-binding environment for the drug under several structural contexts. Because Site III is recognized as a binding region for multiple endogenous and exogenous ligands, including bilirubin, hemin, fusidic acid, and related compounds[13], the present findings raise the possibility that occupancy of this region could influence the local binding environment accessible to RPV under specific physiological or polypharmacy conditions. These results also suggest that the preferred binding landscape is context-dependent, since direct occupation of subdomain IB by bilirubin redistributed favorable poses toward alternative regions, particularly Site II and an adjacent surface-accessible interface. Accordingly, the present study should be interpreted as providing a structural rationale for considering potential Site III-associated competition, rather than as direct evidence of clinically meaningful displacement or a predictor of a specific pharmacokinetic outcome *in vivo*.

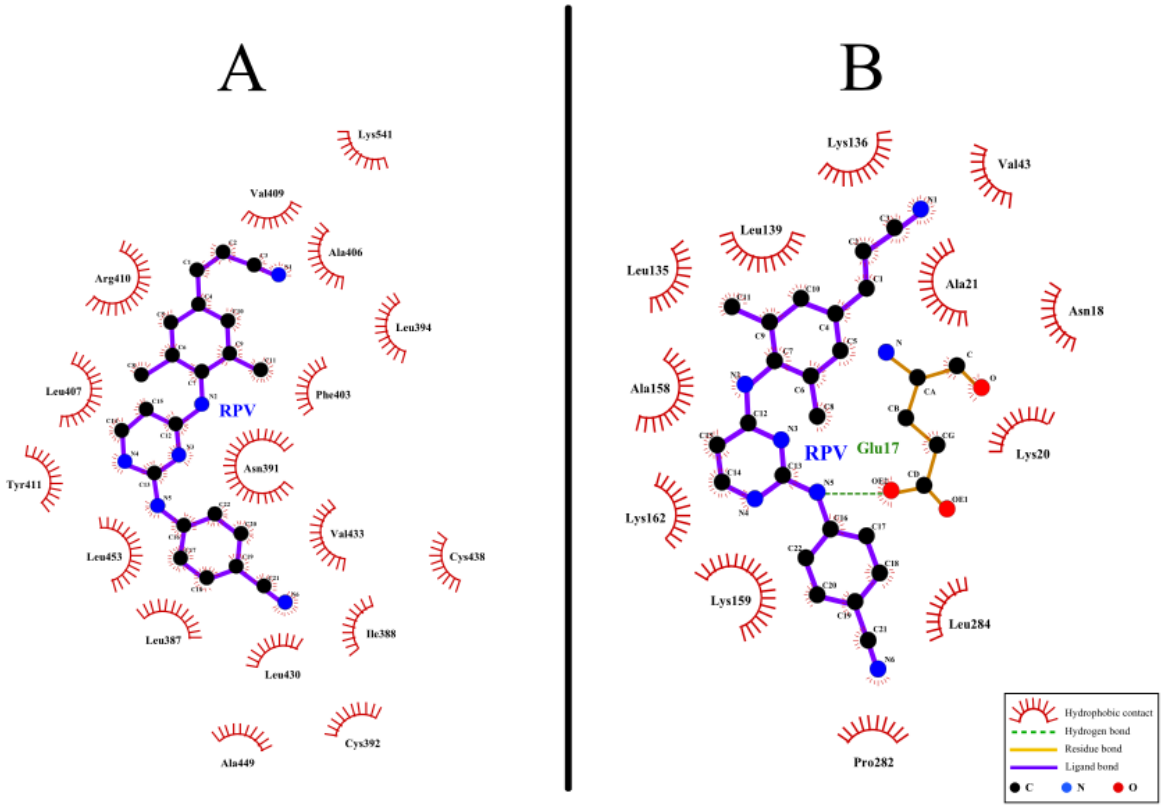

Fig. 9 – Two-dimensional interaction diagrams of representative docked poses of RPV on bilirubin-bound HSA (PDB ID: 2VUE), generated using LigPlot+: A**)** Docked pose of RPV at Sudlow's Site II (subdomain IIIA), showing surrounding protein residues involved in hydrophobic contacts; B**)** Alternative docked pose located near the IA/IB interface adjacent to the bilirubin-binding region, illustrating hydrophobic contacts and a hydrogen bond between RPV and Glu17. Hydrophobic contacts are indicated by red arcs, hydrogen bonds by green dashed lines, ligand covalent bonds by purple lines, and protein residue bonds by yellow lines. Atom types are color-coded (carbon, black; nitrogen, blue; oxygen, red).

Molecular Dynamics Simulation of the RPV–HSA Site III Complex

To assess the dynamic stability of the binding mode identified from docking, a 100 ns molecular dynamics (MD) simulation was performed for the RPV-HSA complex corresponding to the Site III pose in the ligand-free HSA structure (1BM0). This simulation was designed to evaluate the stability of the docked complex under explicit solvent conditions and to characterize the time-dependent behavior of the ligand-protein system. Trajectory analyses focused on global protein stability, residue-level flexibility, overall system stability, and the persistence of ligand-protein contacts.

The RMSD profiles derived from the 100 ns RPV-HSA trajectory are shown in Fig. 10A, which include the HSA backbone (protein-only), the overall complex, and the ligand (RPV). After an initial equilibration period, protein backbone RMSD stabilized and fluctuated within a narrow range over the remainder of the simulation, indicating no progressive structural drift. The complex RMSD remained slightly higher than the protein-only trace, consistent with inclusion of the bound ligand and associated local adjustments rather than large-scale rearrangement. In addition, the ligand RMSD remained low and did not show a sustained upward trend, supporting a consistent ligand pose relative to the protein after equilibration.

Global protein compactness was evaluated by monitoring the radius of gyration (Rg) (Fig. 10B). The Rg remained stable with only minor fluctuations around a constant mean value, indicating that RPV binding did not induce large-scale expansion or compaction of the HSA structure. This behavior suggested preservation of the characteristic albumin fold upon ligand association. Residue-level flexibility was examined using Cα RMSF analysis (Fig. 10C). Elevated fluctuations were primarily confined to surface-exposed loops and terminal regions, while the protein core remained comparatively rigid. Importantly, residues lining the Site III binding region did not display anomalous flexibility relative to the remainder of the protein, indicating that

ligand binding was accommodated without localized destabilization of the pocket. The overall energetic stability of the simulated system was assessed by monitoring the total potential energy as a function of time (Fig. 10D). After an initial equilibration phase, the total energy fluctuated around a stable mean value without systematic drift, indicating that the system remained well equilibrated and numerically stable over the full simulation period.

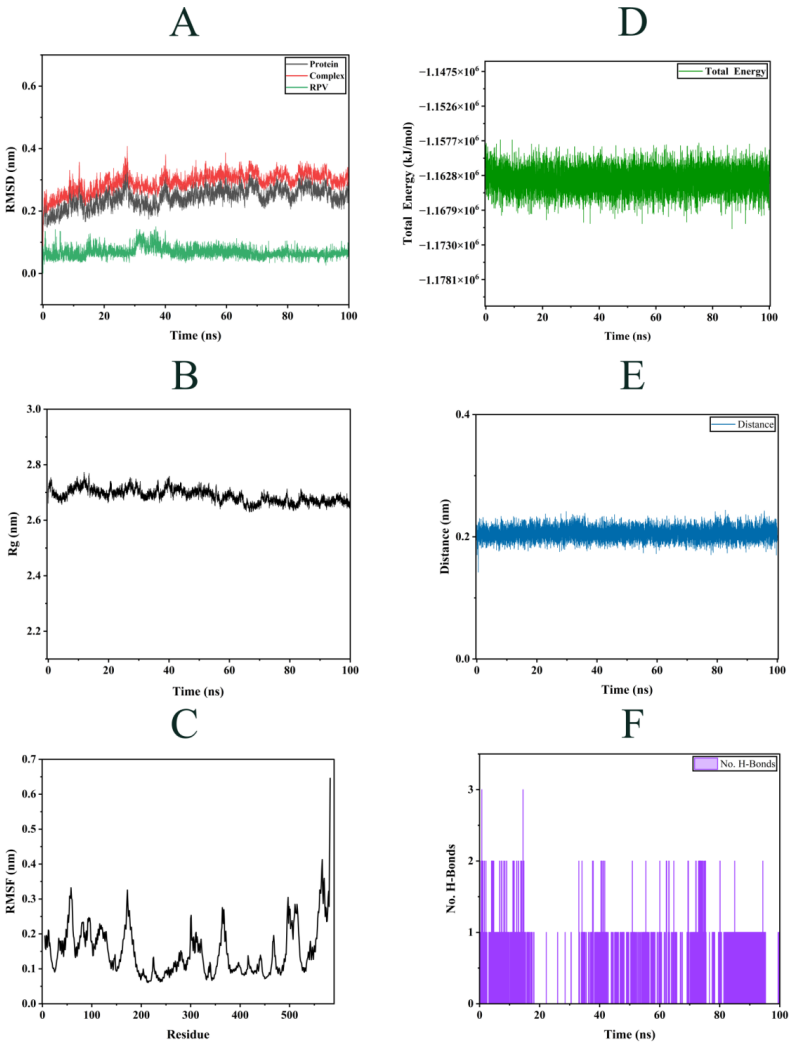

Fig. 10 – Molecular dynamics stability and interaction analysis of the RPV-HSA complex at Site III over a 100 ns simulation: A) Backbone RMSD of free HSA (black) and the RPV-HSA complex (red); B) Radius of gyration (Rg) of HSA throughout the simulation period; C) RMSF profile of HSA residues; D) Total potential energy of the system as a function of time; E) Minimum distance between RPV and HSA over time; F) Time evolution of ligand-protein hydrogen bonds.

Binding persistence was further evaluated by calculating the minimum distance between RPV and HSA as a function of time (Fig. 10E). The ligand-protein distance remained consistently low throughout the simulation, with no excursions indicative of ligand escape into the solvent. In addition, analysis of protein–ligand hydrogen bonds (Fig. 10F) revealed intermittent but recurrent hydrogen-bond formation over the trajectory. Although limited in number, these interactions recur throughout the simulation and contribute to stabilization of the complex in conjunction with hydrophobic contacts. A structural overlay of representative RPV conformations extracted at 0, 20, 40, 60, 80, and 100 ns is shown in Fig. 11. The superposed ligand positions demonstrated that RPV remained confined within the Site III cavity over the entire simulation while sampling multiple orientations within the pocket. No systematic directional drift toward solvent exposure was observed. Taken together, these observations indicated that the Site III binding mode identified by docking corresponded to a dynamically stable and adaptable association over the simulated timescale.

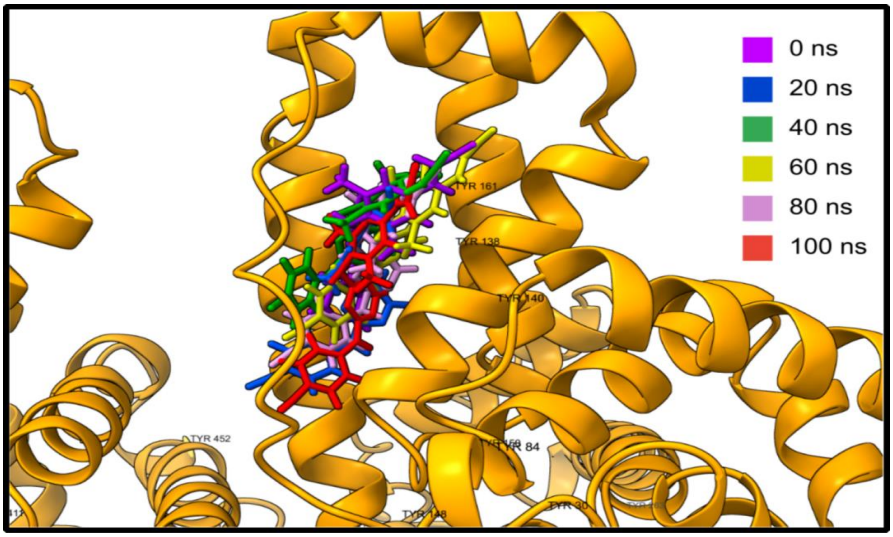

Fig. 11 – Overlay of representative RPV conformations extracted at 0, 20, 40, 60, 80, and 100 ns from the MD trajectory, shown relative to the 0 ns protein reference structure.

CONCLUSION

In this study, comparative molecular docking and molecular dynamics simulations were used to examine plausible binding modes of RPV on HSA under ligand-free and multiple ligand-occupied structural contexts. Docking pose clustering indicated that Site III (subdomain IB) provided consistently favorable and convergent binding energetics for RPV in ligand-free HSA as well as in the warfarin- and diazepam-bound structures, whereas bilirubin occupancy reshaped the accessible binding landscape, redirecting RPV toward Sudlow's Site II or adjacent surface-accessible regions rather than the canonical Site III pocket. These observations underscore that docking results obtained from ligand-bound albumin structures should be interpreted as reflecting local accommodation within constrained binding environments rather than definitive competitive displacement. Molecular dynamics analysis of the Site III complex in ligand-free HSA over 100 ns supported overall protein structural stability and sustained ligand association with the binding cavity. RPV remained confined within the Site III pocket while undergoing orientational and positional adjustments, consistent with a dynamically adaptive binding mode characteristic of drug-albumin interactions. Taken together, these findings supported Site III as a reproducible and permissive region for RPV accommodation across multiple HSA structural contexts when this region remained unoccupied, while highlighting the sensitivity of predicted binding behavior to ligand occupancy. This work provides a cautious computational basis for guiding future displacement experiments and spectroscopic studies aimed at resolving binding-site preference and interaction determinants of RPV–albumin association.

Acknowledgements. This work was supported by a Research Grant (REIG-FPS-2025/036) from UCSI University. The authors thank both Universiti Malaya and UCSI University for providing necessary facilities to carry out this work.

REFERENCES

1. World Health Organization, "HIV and AIDS", World Health Organization, Geneva, 2025, https://www.who.int/news-room/ fact-sheets/detail/hiv-aids
2. UNAIDS, "Fact Sheet 2025: Global HIV Statistics", Joint United Nations Programme on HIV/AIDS, Geneva, 2025, https://www.unaids.org/en/resources/fact-sheet
3. I. Usach, V. Melis and J. E. Peris, *J. Int. AIDS Soc.*, **2013**, *16*, 18567. doi:10.7448/IAS.16.1.18567.
4. U.S. Food and Drug Administration, "EDURANT® (rilpivirine) tablets, for oral use; EDURANT® PED (rilpivirine) tablets, for oral suspension. Highlights of Prescribing Information", U.S. Food and Drug Administration, Silver Spring, 2024, https://www.accessdata.fda.gov/drugsatfda_docs/label/2022/202022s0191bl.pdf
5. D. Hodge, D.J. Back, S. Gibbons, S.H. Khoo, C. Marzolini, *Clin. Pharmacokinet.*, **2021**, *60*, 835–853, https://doi.org/10.1007/s40262-021-01005-1
6. M. Sanford, *Drugs*, **2012**, *72*, 525–541. doi:10.2165/11208590-000000000-00000.
7. European Medicines Agency, "Edurant, INN-rilpivirine", European Medicines Agency, Amsterdam, 2024. https://www.ema.europa.eu/en/documents/product-information/edurant-epar-product-information_en.pdf
8. K. Yamasaki, V. T. G. Chuang, T. Maruyama and M. Otagiri, *Biochim. Biophys. Acta*, **2013**, *1830*, 5435–5443. doi:10.1016/j.bbagen.2013.05.005.

9. G. Fanali, A. di Masi, V. Trezza, M. Marino, M. Fasano and P. Ascenzi, *Mol. Aspects Med.*, **2012**, *33*, 209–290. doi:10.1016/j.mam.2011.12.002.
10. X. M. He and D. C. Carter, *Nature*, **1992**, *358*, 209–215. doi:10.1038/358209a0.
11. G. Sudlow, D. J. Birkett and D. N. Wade, *Mol. Pharmacol.*, **1975**, *11*(6), 824–832. doi: 10.1016/S0026-895X(25)10691-3.
12. S. Curry, *Drug Metab. Pharmacokinet.*, **2009**, *24*, 342–357. doi:10.2133/dmpk.24.342.
13. F. Zsila, *Mol. Pharm.*, **2013**, *10*, 1668–1682. doi:10.1021/mp400027q.
14. J. Ghuman, P. A. Zunszain, I. Petitpas, A. A. Bhattacharya, M. Otagiri and S. Curry, *J. Mol. Biol.*, **2005**, *353*, 38–52. doi:10.1016/j.jmb.2005.07.075.
15. C. Coppinger and P. L. Anderson, Expert Opin. Drug Metab. Toxicol., 2025, 21, 343–346. doi:10.1080/ 17425255.2024.2448970
16. K. Vuignier, J. Schappler, J. -L. Veuthey, P. A. Carrupt and S. Martel, *Anal. Bioanal. Chem.*, **2010**, *398*, 53–66. doi:10.1007/s00216-010-3737-1.
17. E. Gayathiri, P. Prakash, S. Y. Chaudhari, S. Sabarathinam, S. D. Priyadharshini, M. K. Al-Sadoon *et al*., Energy Nexus, 2025, 17, 100351. doi:10.1016/ j.nexus.2024.100351
18. M. Yildiz, *J. Mol. Recognit.*, **2024**, *37*, e3105. doi:10.1002/jmr.3105.
19. H. M. Berman, J. Westbrook, Z. Feng, G. Gilliland, T. N. Bhat, H. Weissig *et al*. *Nucleic Acids Res.*, **2000**, *28*, 235–242. doi:10.1093/nar/28.1.235.
20. S. Sugio, A. Kashima, S. Mochizuki, M. Noda and K. Kobayashi, *Protein Eng.*, **1999**, *12*, 439–446. doi:10.1093/ protein/12.6.439.
21. P. A. Zunszain, J. Ghuman, A. F. McDonagh and S. Curry, *J. Mol. Biol.*, **2008**, *381*, 394–406. doi:10.1016/j.jmb.2008.06.016.
22. G. M. Morris, R. Huey, W. Lindstrom, M. F. Sanner, R. K. Belew, D. S. Goodsell *et al*., *J. Comput. Chem.*, **2009**, *30*, 2785–2791. doi:10.1002/jcc.21256.
23. M. D. Hanwell, D. E. Curtis, D. C. Lonie, T. Vandermeersch, E. Zurek and G. R. Hutchison, *J. Cheminform.*, **2012**, *4*, 17. doi:10.1186/1758-2946-4-17.
24. OriginPro, version 2025b; OriginLab Corporation, Northampton, MA, **2025**.
25. E. F. Pettersen, T. D. Goddard, C. C. Huang, E. C. Meng, G. S. Couch, T. I. Croll *et al*., *Protein Sci.*, **2021**, *30*, 70–82. doi:10.1002/pro.3235.
26. A. C. Wallace, R. A. Laskowski and J. M. Thornton, *Protein Eng.*, **1995**, *8*, 127–134. doi:10.1093/protein/8.2.127.
27. M. J. Abraham, T. Murtola, R. Schulz, S. Páll, J. C. Smith, B. Hess *et al*., *SoftwareX*, **2015**, *1–2*, 19–25. doi:10.1016/j.softx.2015.06.001.
28. R. B. Best, X. Zhu, J. Shim, P. E. M. Lopes, J. Mittal, M. Feig, et al., *J. Chem. Theory Comput.*, **2012**, *8*, 3257–3273. doi:10.1021/ct300400x.
29. W. L. Jorgensen, J. Chandrasekhar, J. D. Madura, R. W. Impey and M. L. Klein, *J. Chem. Phys.*, **1983**, *79*, 926–935. doi:10.1063/1.445869.
30. V. Zoete, M. A. Cuendet, A. Grosdidier and O. Michielin, *J. Comput. Chem.*, **2011**, *32*, 2359–2368. doi:10.1002/jcc.21816.
31. G. Bussi, D. Donadio and M. Parrinello, *J. Chem. Phys.*, **2007**, *126*, 014101. doi:10.1063/1.2408420.
32. M. Parrinello and A. Rahman, *J. Appl. Phys.*, **1981**, *52*, 7182–7190. doi:10.1063/1.328693.
33. T. Darden, D. York and L. Pedersen, *J. Chem. Phys.*, **1993**, *98*, 10089–10092. doi:10.1063/1.464397.